Applied Catalysis B: Environmental 232 (2018) 384–390

Contents lists available at ScienceDirect

Applied Catalysis B: Environmental

journal homepage: www.elsevier.com/locate/apcatb

Porous carbon nitride with defect mediated interfacial oxidation for improving visible light photocatalytic hydrogen evolution

Zhao Zhang[a], Luhua Lu[a,b,*], Zaozao Lv[a], Ying Chen[a,b], Hongyun Jin[a], Shuen Hou[a], Lixin Qiu[c], Limei Duan[c], Jinghai Liu[c,**], Kai Dai[d]

[a] Faculty of Materials Science and Chemistry, China University of Geosciences Wuhan, 388 Lumo Road, Wuhan 430074, PR China
[b] Zhejiang Institute, China University of Geosciences Wuhan, Hangzhou, 311305, PR China
[c] Inner Mongolia Key Laboratory of Carbon Nanomaterials, College of Chemistry and Chemical Engineering, Inner Mongolia University for Nationalities, Tongliao, 028000, PR China
[d] College of Physics and Electronic Information, Huaibei Normal University, Huaibei, 235000, PR China

ARTICLE INFO

Keywords:
Graphitic carbon nitride
Defects
Porous
Interfacial oxidation
Photocatalytic hydrogen evolution

ABSTRACT

The Feasibility of interfacial redox reaction has determinant role in hydrogen evolution during photocatalytic water-splitting process. Here, we report that promoting interfacial oxidation ability of porous graphitic carbon nitride (Pg-C_3N_4) with defects can effectively improve visible light photocatalytic hydrogen evolution (PHE) activity. Pg-C_3N_4 with edge site defects was fabricated by constraining growth of g-C_3N_4 on porous kaolinite-derived template. The Pg-C_3N_4 with extra electrons of defects caused by enriched basal plane holes exhibits higher electrocatalytic activity for oxidation process in comparison with reduction process. This feature benefits electron-transfer reaction to quench photo-excited holes during photocatalysis process and promote photo-electrons reaction, which was proved by photoluminescence spectra of Pg-C_3N_4 and g-C_3N_4 and different PHE activity variation of their heterojunction materials with TiO_2. The results show that PHE rate for Pg-C_3N_4 reaches 1917 $umol^{-1}\ g^{-1}\ h^{-1}$, 2.37 times of g-$C_3N_4$ under visible light irradiation. This approach of engineering interfacial defects to accelerate hole's oxidation reactions during photocatalytic water-splitting would advance two-dimensional (2D) catalysis for solar fuel production.

1. Introduction

Photocatalytic hydrogen evolution (PHE) by water-splitting half-reaction with semiconductor photocatalysts has been recognized as a clean energy production approach [1]. To produce hydrogen via photocatalytic approach, sufficient conduction band potential (CBP) of semiconductor materials is needed to provide overpotential for hydrogen evolution. Graphitic carbon nitride (g-C_3N_4) with CBP at −1.24 V with respect to normal hydrogen electrode potential (NHE) and narrow band-gap has been employed as a metal-free photocatalyst for water-splitting to H_2 under visible light irradiation [2,3]. The chemical inert character of g-C_3N_4 endows it with stable cyclic photocatalytic performance. However, photocatalytic activity of g-C_3N_4 under visible light is very low in comparison to other semiconductor nanomaterials such as metal oxides [4,5], metal oxynitrides [6], and metal sulphides [7]. It is considered that the structural defects of g-C_3N_4 would localize photo-generated polarons and accelerate their recombination, which prohibits the production and transfer of interfacial free electrons to produce hydrogen. Guided by this idea, intensive researches [8–16] have thus been done to increase visible light absorption by narrowing the band-gap, to improve charge separation by constructing heterojunctions, increase surface hydrogen evolution sites by increasing specific surface area (SSA) and introduce cocatalyst such as Pt [17], AuPd [18], WS_2 [19], MoS_2 [20], CoS [21], NiP [22] and Ni/NiO [23].

Generally, PHE reaction involves three major steps: (i) light absorption by semiconductor photocatalysts to generate electron-hole pairs, (ii) charge separation and migration to surface active sites, (iii) interfacial reactions for reduction of protons to H_2 and oxidation of OH^- (for full water splitting) or sacrificial electron donors (for half-reaction). The first two steps are related to fast photoelectrical process along with the third step of electrochemical process. During this electrochemical reaction process, both reduction reaction (electrons reactions) and oxidation reaction (holes reactions) are spontaneous process on the interface and the slow one is considered as the rate-determined step with large overpotential. Therefore, tremendous attentions have

* Corresponding author at: Faculty of Materials Science and Chemistry, China University of Geosciences Wuhan, 388 Lumo Road, Wuhan 430074, PR China.
** Corresponding author.
E-mail addresses: lhlu@cug.edu.cn (L. Lu), jhliu2015@imun.edu.cn (J. Liu).

https://doi.org/10.1016/j.apcatb.2018.03.086
Received 12 September 2017; Received in revised form 28 February 2018; Accepted 24 March 2018
Available online 26 March 2018
0926-3373/ © 2018 Elsevier B.V. All rights reserved.

been paid on exploring hydrogen evolution active sites provided by co-catalysts such as platinum (Pt), which serves as an electron sink with suitable hydrogen absorption free energy [17]. However, protons reduction by electrons would be suppressed if holes reaction on the interface is slow [24]. To well understand PHE process on the g-C_3N_4, it is necessary to investigate the interfacial hole reaction activity. Recently, research has shown that addition of K_2HPO_4 facilitates hole oxidation kinetics that dramatically improve hydrogen evolution activity on g-C_3N_4 nanosheets [25]. Besides, decorating hole reaction cocatalyst CoP on Pt-g-C_3N_4 further increase hydrogen evolution due to the increased oxygen evolution rate [26]. Although these research have achieved important progress, little attentions have been focus on investigating the effects of intrinsic structure of g-C_3N_4 on hole reaction kinetics during PHE process.

Herein, we report a defect rich porous g-C_3N_4 (Pg-C_3N_4) obtained by confined pyrolysis of urea on porous hard template obtained by modification of natural nanomaterial kaolinite. Pg-C_3N_4 with rich edge site defects have shown obviously enhanced PHE activity under visible light irradiation. Electrochemical analysis has shown that interfacial oxidation activity of Pg-C_3N_4 is much higher than that of g-C_3N_4, while keeping the same interfacial reaction activity towards protons reduction. Interfacial junction construction along with photocurrent analysis also demonstrate that defects on Pg-C_3N_4 present excellent capability to mediate hole reaction towards interfacial oxidation and photocurrent increase.

2. Experimental

2.1. Preparation

To prepare porous hard template, 50 g kaolinite powder was annealed at 850 °C in air atmosphere for 2 h to transfer it into amorphous metal kaolinite. Then annealed powder was stirred in 300 mL 2 M HCl overnight twice followed by washing with 2 L deionized water and drying at 80 °C to remove Al_2O_3 phase obtaining a porous product composed of amorphous SiO_2. Then, 10 g urea (AR, Sinopharm Chemical Reagent Co., Ltd) was mixed with 20 g porous template and placed in a covered corundum crucible and heated to 550 °C with temperature increase rate of 10 °C/min and preserved for 3 h in air atmosphere and naturally cooled to room temperature in a tube furnace. Then, the sample was washed with 100 mL HF (10%) third times at 60 °C 100 mL nitric acid (0.1 mol L^{-1}) and 1 L distilled water (DI water) to remove SiO_2 and other impurities followed by filtering and drying at 80 °C to obtain Pg-C_3N_4. g-C_3N_4 was synthesized without template in the same thermal treatment program without HF washing. Pt loaded Pg-C_3N_4 (or g-C_3N_4) was obtained by photodeposition. 0.3 mL $H_2PtCl_6 \cdot 6H_2O$ (10 mg mL^{-1}, AR, Sinopharm Chemical Reagent Co., Ltd) and 2 mL acetic acid (1 mol L^{-1}, Sinopharm Chemical Reagent Co., Ltd) were added into 100 mL g-C_3N_4 dispersion (1 mg mL^{-1}) to obtain 3 wt% Pt-g-C_3N_4 (or Pt-Pg-C_3N_4). After N_2 bubbling for an hour to remove the oxygen (O_2) in the system, the sample was irradiated by a 300 W Xe lamp (PLS-SXE 300, Beijing Perfect light Technology Co., Ltd) for three hours. Then, the Pt-g-C_3N_4 (or Pt-Pg-C_3N_4) was obtained by filtering and drying at 80 °C overnight. For preparation of Pt-g-C_3N_4-TiO_2 and Pt-Pg-C_3N_4-TiO_2, the above prepared sample were bath sonicated with TiO_2 (Degussa P25) at mass ratio of 1:9 of TiO_2 to g-C_3N_4 or Pg-C_3N_4 for 1 h in 100 mL deionized water followed by filtration and drying at 80 °C overnight.

2.2. Characterization

All measurement was carried out in 25 °C room temperature environment. Morphology of samples was characterized through TEM (Tecnai G2 F20S-TWIN at 200 kV). Structure analysis was carried out through XRD (Bruker AXS D8-Focus) BET (Micromeritics ASAP2020) and XPS (X'Pert-Pro MPD using Cu Kα (λ = 1.5406 A). UV–vis DRS measurements were carried out using a Hitachi UV-3600 UV–vis spectrophotometer equipped with an integrating sphere attachment. Analysis range was from 200 to 600 nm, and $BaSO_4$ was used as a reflectance standard. PL spectra of photocatalysts were measured by FLS920 with excitation wavelength of 325 nm. The EPR spectra were obtained on a JES-FA 200 EPR spectrometer.

2.3. Hydrogen (H_2) evolution test

Photocatalytic water splitting reactions were carried out in a Pyrex top-irradiation reaction vessel connected to a glass closed gas circulation system. 80 mg Pt loaded catalyst was dispersed in a mixture of 54 mL deionized water and 6 mL triethanolamine (TEOA) (78%, Sinopharm Chemical Reagent Co., Ltd) by sonication for 0.5 h. The obtained reactant dispersion was put into reaction vessel and stirred. Reaction system was evacuated three times with half an hour each time to remove air completely prior to irradiation under a 300 W Xe lamp with water filter. Wavelength of incident light was controlled by using cut-off filters (> 400 nm). The temperature of reactant solution was maintained at room temperature by a flow of cooling water during reaction. Evolved gases were analyzed by gas chromatography (GC 7890II, Shanghai Techcomp Instrument Ltd.) equipped with a thermal conductive detector (TCD) with argon as carrier gas.

2.4. Electrochemical measurements

Electrochemical measurements were carried out on a CHI760E electrochemical work station (Shanghai Chenhua) in three electrodes system. To remove bubbles generated during measurement, rotation speed of electrode has been controlled 1600 rpm by MRS electrode rotator (Pine Research Instrumentation, USA). Typically, 1 mg of catalyst and 10 μl of 5 wt% Nafion solution were dispersed in 1 ml of 6:1(v/v) water/ethanol and sonication for 2 h to form a homogenous solution. 60 μl solution was loaded on a 5-mm-diamter clean glassy carbon rotation disk electrode (mass loading 0.306 mg cm^{-2}) and dried under room temperature. Measurement was carried out in 10% TEOA solution that was used for PHE test, with a Pt wire as counter electrode and reference electrode was Ag/AgCl. LSV measurement was scanned at scan rate of 2 mV s^{-1}. Before measurement, electrolyte solution was bubbled with N_2 and H_2 for 1 h to completely remove O_2 and scanned CV from −1 V to 2 V until a stable curve is achieved.

3. Results and discussion

Synthetic process of Pg-C_3N_4 can be seen in Fig. 1A. The detailed structure variation from raw kaolinite to porous template via thermal annealing and acid washing can be seen in supporting information (See Fig. S1). Pyrolysis of urea on porous template has resulted in uniform deposition of g-C_3N_4 on template surface as has been confirmed via TEM imaging (Fig. 1B and C) and element mapping of C, N, O and Si (Fig. 1D, E, F and G). By removing amorphous phase of SiO_2 via HF washing, Pg-C_3N_4 was obtained. Pg-C_3N_4 has shown large amount of in-plane holes (Fig. 1H). For comparison, g-C_3N_4 (Fig. 1I) synthesized without template has shown no in-plane holes. In accordance with porous structure confirmed by TEM analysis, N_2 adsorption/desorption isotherm curves in Fig. 1J has shown that Pg-C_3N_4 has BET specific surface area of 109 m^2/g, which is much higher than 40 m^2/g of g-C_3N_4. The pore volume distribution of Pg-C_3N_4 and g-C_3N_4 in Fig. 1K has shown increased pore volume of Pg-C_3N_4 over g-C_3N_4 from 2 to 61 nm pore size range. Moreover, a peak at 2.14 nm pore size of Pg-C_3N_4 was found indicating the porous hard template directed synthesis of Pg-C_3N_4 has leaded to smaller pore formation in compared with that of g-C_3N_4 synthesized without template. Thus, template directed synthetic approach of Pg-C_3N_4 endow it large specific surface area along with rich-pore formation.

The structure of Pg-C_3N_4 was probed by X-ray Diffraction (XRD) and

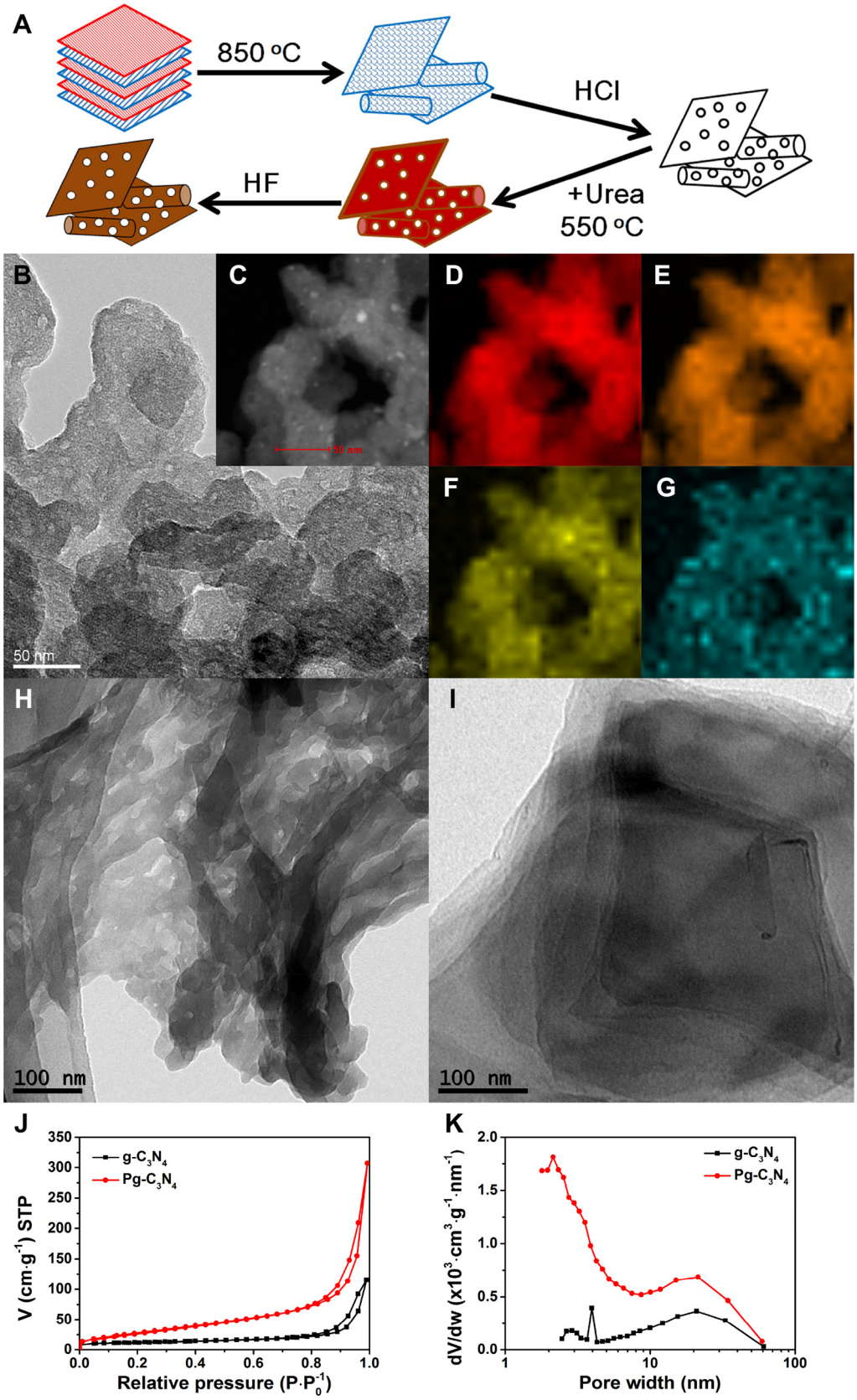

Fig. 1. Morphology and pore structures of Pg-C_3N_4 with rich edges of basal plane holes as defect sites, (A) Schematic illustration of fabrication by confined growth of urea on porous Kaolinite-derived template, (B) TEM image of g-C_3N_4 deposited on porous template, (C) Corresponding STEM image, scale bar 50 nm. Elemental mappings for Carbon (D), Nitrogen (E), Oxygen (F) and Silicon (G), scale bar 50 nm, (H) TEM image of Pg-C_3N_4 after removing template, (I) TEM image for g-C_3N_4 without template, (J) N_2 adsorption/desorption isotherms, (K) BJH pore size distribution.

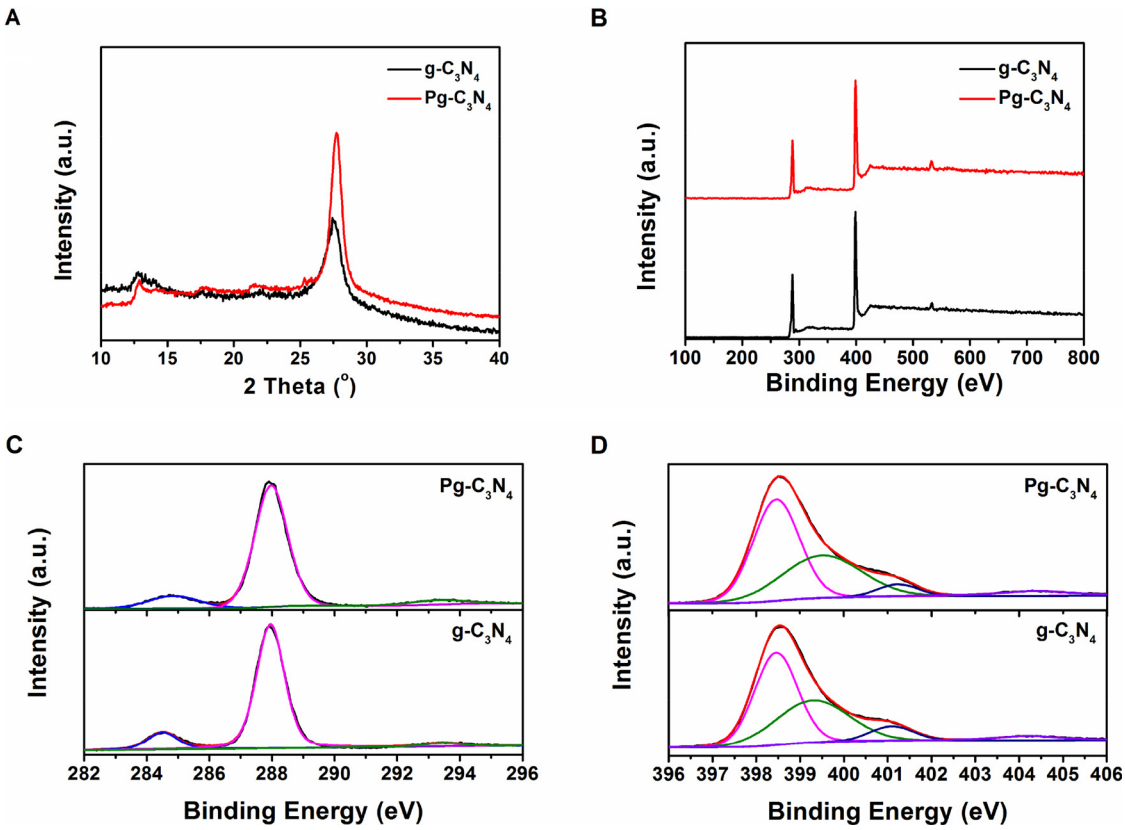

Fig. 2. (A) XRD patterns, (B) XPS survey, High-resolution XPS spectra for (C) C1s and (D) N1s of g-C_3N_4 and Pg-C_3N_4.

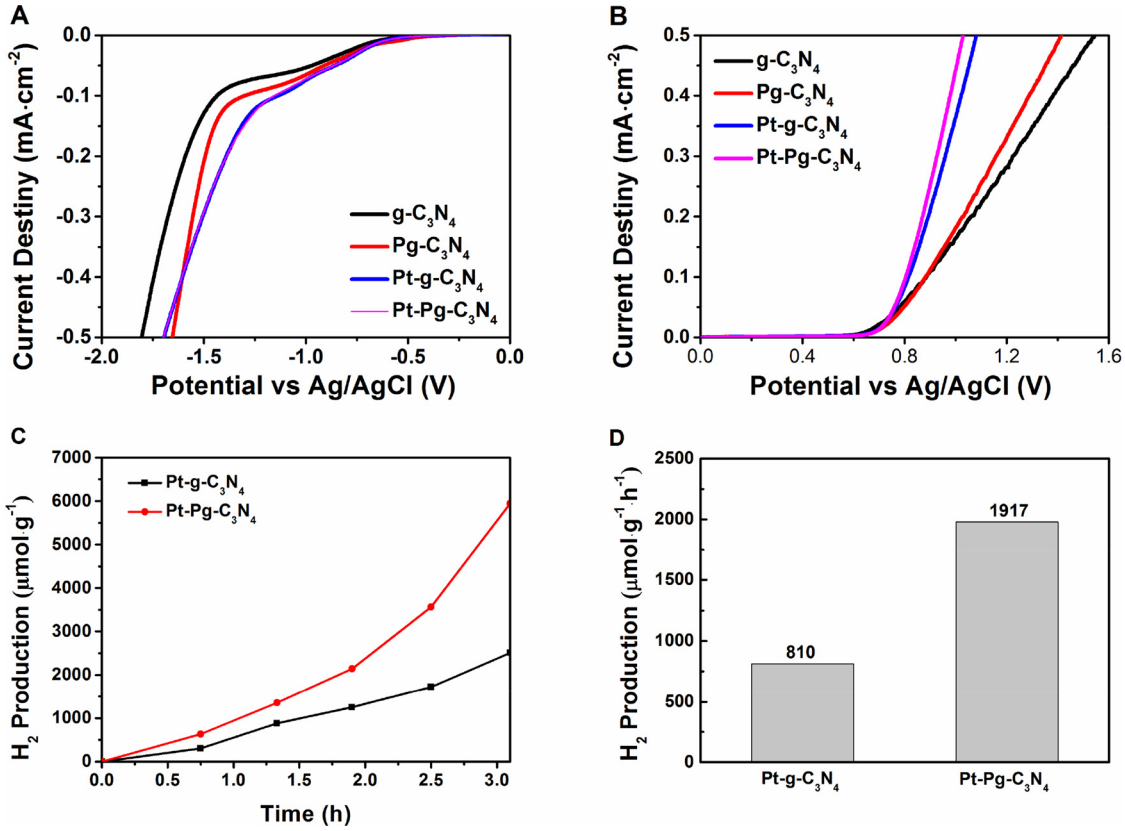

Fig. 3. Pg-C_3N_4 with defect sites promoting interfacial oxidation and photocatalytic hydrogen evolution (PHE). (A) LSV curves of a cathodic scan from 0 to −2 V (vs Ag/AgCl) in TEOA solution. (B) LSV curves of an anodic scan from 0 to 1.6 V (vs Ag/AgCl) in TEOA solution. (C) PHE kinetics under visible light irradiation. (D) Comparison of PHE rate for Pt loaded g-C_3N_4 (Pt-g-C_3N_4) and Pt loaded Pg-C_3N_4 (Pt-Pg-C_3N_4).

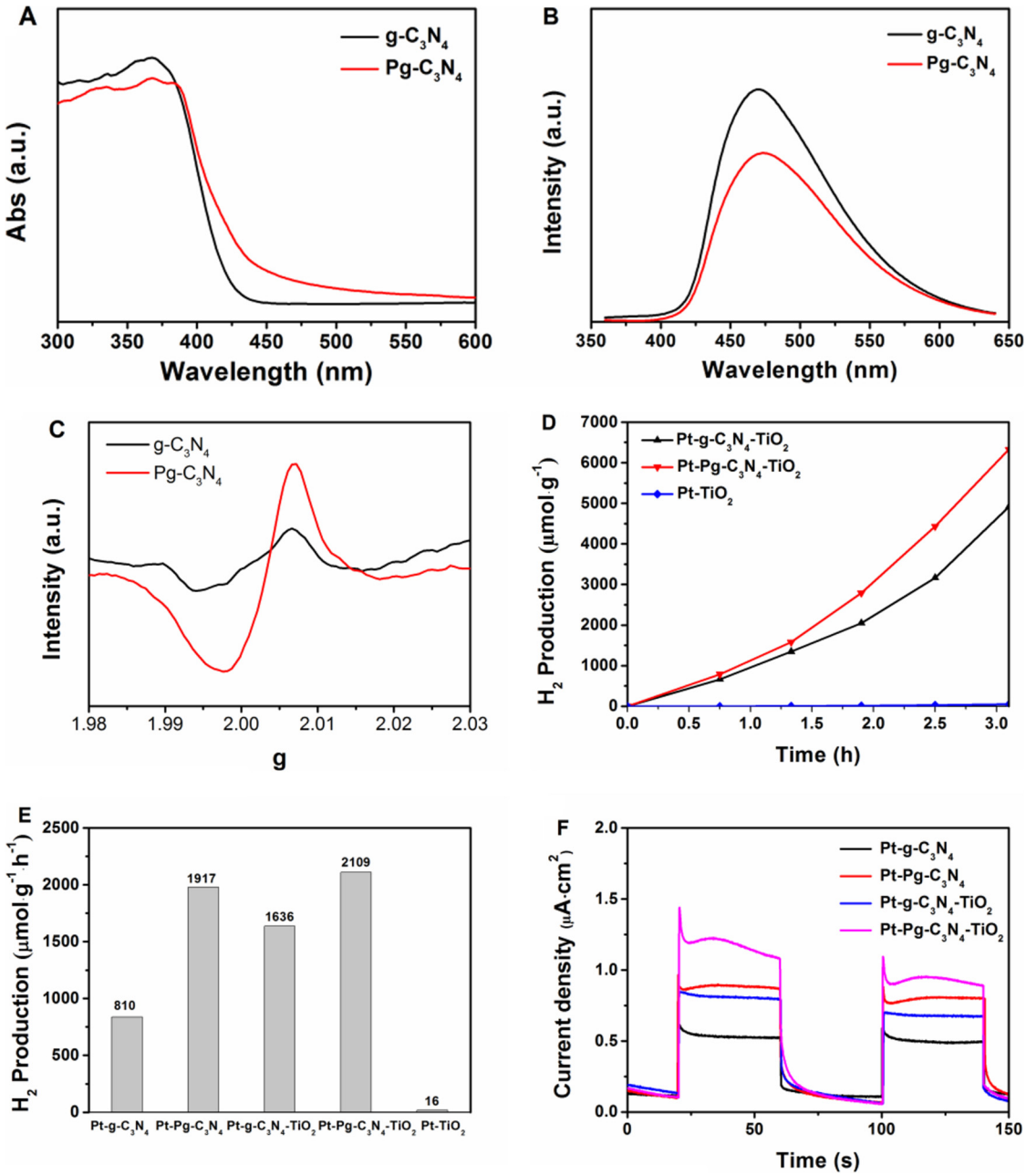

Fig. 4. Photophysical and photocatalytic properties of Pg-C_3N_4 and Pg-C_3N_4-TiO_2. (A) UV-vis DRS, (B) Photoluminescence and (C) EPR spectra for Pg-C_3N_4 and g-C_3N_4. (D) PHE for Pt-Pg-C_3N_4-TiO_2, Pt-g-C_3N_4-TiO_2 and Pt-TiO_2 under visible light irradiation. (E) Hydrogen evolution rate for Pt-g-C_3N_4, Pt-Pg-C_3N_4, Pt-Pg-C_3N_4-TiO_2, Pt-g-C_3N_4-TiO_2 and Pt-TiO_2. (F) Photocurrents of Pt-g-C_3N_4, Pt-Pg-C_3N_4, Pt-Pg-C_3N_4-TiO_2 and Pt-g-C_3N_4-TiO_2.

X-ray photoelectrons spectroscopy (XPS). XRD spectra in Fig. 2A show that Pg-C_3N_4 has typical condensed structure of g-C_3N_4 with in-plane repeating heptazine units (C_6N_7) of diffraction peak at 12.8°. The diffraction peak at 27.7° for layered stacking of Pg-C_3N_4 indicates interlayer space distance of 0.3217 nm, slightly lower than 0.3251 nm of g-C_3N_4 at 27.4°. This may be caused by confined growth of Pg-C_3N_4. XPS survey spectra (Fig. 2B) exhibits C/N atomic ratio of 0.83 for Pg-C_3N_4, which is smaller than the one of 0.85 for g-C_3N_4 synthesized without template. High-resolution C1s and N1s spectra in Fig. 2C and 2D show typical chemical bonds of sp^2-bonded carbon (N—C═N) at 288.01 eV, sp^2 hybridized aromatic N bonded to carbon atoms (C═N—C) at 398.4 eV and tertiary N bonded to carbon at 399.6 eV [27], similar to g-C_3N_4 without templates. Since synthesized graphitic carbon nitride materials are not of perfect structure, there are inevitable structure defects in the basal plane of them. For example, the synthesized graphitic carbon nitrides inevitably contain residual oxygen. The residual oxygen in Pg-C_3N_4 has been found to be 3.76 at% in comparison to that of 1.96 at% in g-C_3N_4, which provide an evidence for influence of template surface on oxygen of Pg-C_3N_4. It can be found that increased residual oxygen has increased bond intensity of O—C═O and N-Oxide at 293.4 and 401.5 eV respectively. Previous research has shown similar phenomenon for g-C_3N_4 synthesized on SiO_2 nanosphere template [28].

To demonstrate roles of defect sites caused by basal plane holes for promoting interfacial oxidation and photocatalytic hydrogen evolution (PHE), we have investigated electrochemical behaviors and photocatalytic activity of Pg-C_3N_4 and Pt-Pg-C_3N_4 along with g-C_3N_4 and Pt-g-C_3N_4 in triethanolamine (TEOA) solution, which was used for PHE. Result in Fig. 3A exhibits similar reduction curves for Pg-C_3N_4 and g-C_3N_4, where the small current density across cathodic potentials to

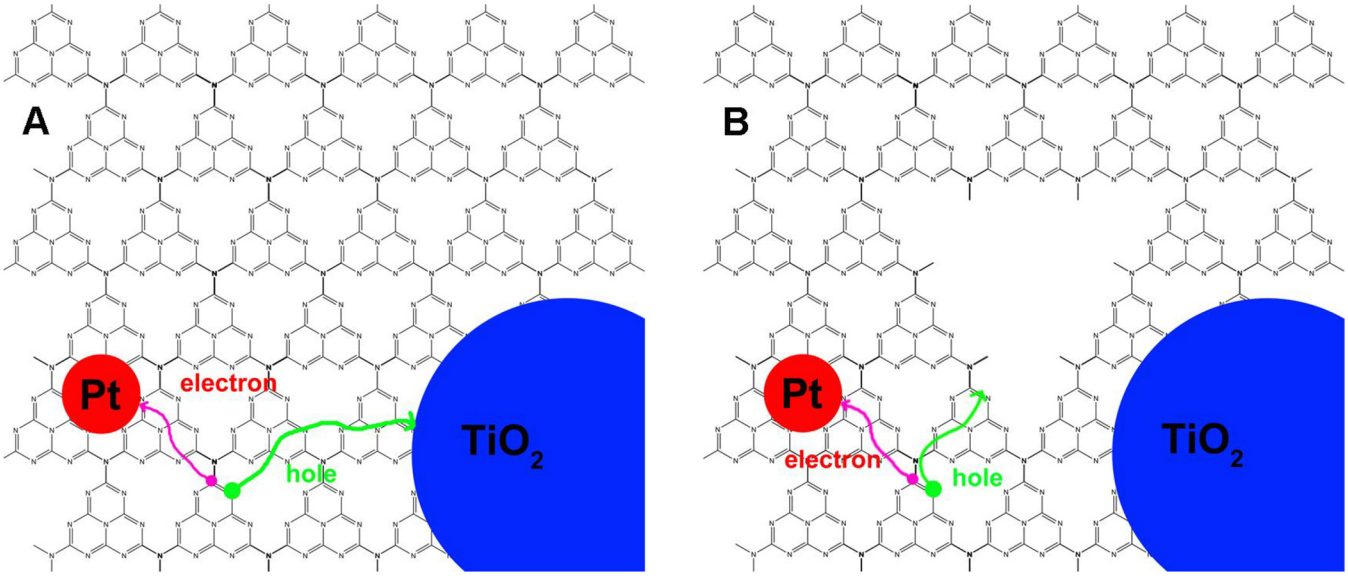

Scheme 1. Illustration for photo-generated electron and hole transportation on Pt-g-C_3N_4-TiO_2 and Pt-Pg-C_3N_4-TiO_2.
Based on above analysis, we can explain the mecha

−1.5 V (vs Ag/AgCl) is attributed to capacitive behaviors. Then, a large current density of hydrogen evolution occurs at the onset potential of −1.5 V (vs Ag/AgCl). The increase of current density for Pg-C_3N_4 during cathodic LSV process should be due to the defects. Interestingly, we observed that onset potential of hydrogen evolution moved to −1.2 V (vs Ag/AgCl) after Pt loading for Pg-C_3N_4 and g-C_3N_4. And, both LSV cathodic curves coincide, indicating the same hydrogen evolution activity. The anodic curves for oxidation of triethanolamine (TEOA) in Fig. 3B show the same onset potential for Pg-C_3N_4 and g-C_3N_4 at 0.7 V (vs Ag/AgCl). But, anodic currents for Pg-C_3N_4 Pt-Pg-C_3N_4 are 1.12 and 1.2 times larger than of g-C_3N_4 and Pt-g-C_3N_4 at 1 V (vs Ag/AgCl) respectively, indicating important role of defects on promoting hole reaction [29]. These results denote that defects at Pt-Pg-C_3N_4 depress electron and hole recombination via enhanced hole reaction activity with TEOA and facilitates reduction of H_2O to H_2.

Contribution of defect sites for promoting photocatalytic hydrogen evolution (PHE) was evaluated under visible light with TEOA as sacrificial donors. The results in Fig. 3C and D have shown that hydrogen evolution of Pt-Pg-C_3N_4 reaches to 5943 μmol g^{-1} after 3.1 h irradiation, which is 2.37 times of Pt-g-C_3N_4 (2511 μmol g^{-1}). And hydrogen evolution rate of Pt-Pg-C_3N_4 is 1917 $\mu mol^{-1}\, g^{-1}\, h^{-1}$. Moreover, direct evidence has also been observed from PHE of g-C_3N_4 and Pg-C_3N_4 without loading Pt (Fig. S2). Since lack of surface active sites of catalysts for hydrogen evolution would reduce their PHE yield, PHE measurement was conducted for longer time to show defects enhanced PHE of Pg-C_3N_4 over that of g-C_3N_4 under visible light irradiation. Beside, cyclic PHE measurement and according XRD patterns of Pg-C_3N_4 before and after cyclic measurement have shown its good PHE and phase stability (Fig. S3). These results indicate increased PHE activity would be due to structural defects on in-plane sheet of Pg-C_3N_4, where defects facilitate hole transfer to accelerate its reactivity.

Beside interface redox activity, photophysical characters of catalysts have also been measured. UV–Vis DSR spectra in Fig. 4A shows that absorption edge of Pg-C_3N_4 has been extended to 470 nm in comparison to that of g-C_3N_4, and band-gap of Pg-C_3N_4 has found to be 2.63 eV in compared to 2.95 eV of g-C_3N_4 based on the relationship of for absorption edge (A.E.) and band-gap (Eg). Photoluminescence (PL) spectra in Fig. 4B exhibits a decreased PL emission Pg-C_3N_4, indicating defects in g-C_3N_4 would affect electronic structures and kinetics of excited states to reduce recombination of photo-generated electrons and holes [29]. Since rich edges around basal plane holes may induce extra electrons in Pg-C_3N_4, Electron paramagnetic resonance (EPR) spectra have been measured. As has been shown in Fig 4C, the EPR spectra of Pg-C_3N_4 displays a strong symmetrical signal centering at g = 2.0036, indicating lone electron pair on the carbon atoms of the heptazine rings. Pg-C_3N_4 has shown greater ability to delocalize electrons by structure defects than g-C_3N_4 without basal plane holes [30–35]. To further demonstrate enhanced hole reaction that facilitate charge separation in Pg-C_3N_4 during PHE process, we applied the concept in solar cell design that utilizing hole transfer materials at heterojunction interface to suppress combination of photogenerated electrons and holes. In our case, we employed titanium dioxide (TiO_2) as hole transfer material to construct interfacial junction with g-C_3N_4 [36–38], then examined PHE activity by comparison of differences between defects and TiO_2 hole transfer junction for PHE. PHE activities for composites with interfacial junctions are present in Fig. 4D and E. Pt-TiO_2 shows negligible PHE activity under visible light, indicating no contribution from TiO_2 due to unexcited wide band-gap. Pt-Pg-C_3N_4-TiO_2 exhibits yield of hydrogen of 6328 μmol g^{-1}, only 1.06 times of Pt-Pg-C_3N_4. In comparison, Pt-g-C_3N_4-TiO_2 presents yield of 4910 μmol g^{-1}, 1.96 times of Pt-g-C_3N_4. These results indicate that interfacial junction between g-C_3N_4 and TiO_2 provide much more contributions to hole transfer than pure g-C_3N_4 interface mediating hole reaction for oxidation of TEOA towards accelerating the separation of photo-generated electrons and holes. Photocurrent results in Fig. 4F also confirm fact that defects on Pt-Pg-C_3N_4 and interfacial junctions with TiO_2 increase photogenerated free electrons release. Thus, limited contributions of Pg-C_3N_4-TiO_2 interfacial junctions to PHE strongly demonstrate that defects on Pg-C_3N_4 present excellent capability to mediate hole reaction towards interfacial oxidation as has been shown in Scheme 1.

Based on above analysis, we can explain the mechanism of enhanced PHE activity of Pg-C_3N_4 over g-C_3N_4. Pg-C_3N_4 with defective porous structure was found to have extra electrons in defects, which is caused by formation of basal plane holes and conformed by EPR spectra analysis. Pg-C_3N_4 with extra electrons exhibits higher interfacial oxidation activity over that of g-C_3N_4. Beside enhanced charge separation of Pg-C_3N_4 by its defect structure, which was proved via photoluminescence spectra analysis, Pg-C_3N_4 with enhanced interfacial oxidation activity can further prohibit recombination of photo-generated electrons and holes. The PHE activity variation from Pg-C_3N_4 and g-C_3N_4 to their composites with TiO_2, which provides extra heterojunction interfacial to capture accumulated holes, has shown prohibited

accumulation of hole in Pg-C_3N_4 during PHE process in compared with g-C_3N_4 and their composites with TiO_2. The effective consumption of holes via enhanced interfacial oxidation activity reflected by prohibited accumulation of hole in Pg-C_3N_4 has thus been attributed to the mechanism of enhanced PHE activity of Pg-C_3N_4.

4. Conclusions

In conclusion, we have fabricated a porous g-C_3N_4 with in-plane holes by constrained pyrolysis of urea on a porous kaolinite-derived template. The basal plane holes of porous g-C_3N_4 provide high specific surface area, extended light absorption, and defect as active sites for mediating hole reactivity towards interfacial oxidation. And, we also demonstrate the contribution of interfacial hole reactivity including hole transfers and hole electrochemical reactions to photocatalytic hydrogen evolution of g-C_3N_4. This work provide an approach of defects design to mediate the interfacial oxidation reaction for promoting photocatalytic hydrogen evolution activity of catalysts.

Acknowledgements

This work was supported by the National Key Research Program of China (2016YFA0201001), National Natural Science Foundation of China (21303129, 21303080 and 51102218), Fundamental Research Funds (CUG140620 and CUGL150413) for the Central Universities, China University of Geosciences (Wuhan) and Natural Science Foundation of Zhejiang Province, China (LZ16E020001), Program for Young Talents of Science and Technology in Universities of Inner Mongolia Autonomous Region (NJYT-15-B14), Program for the Top Young Innovative Talents of Inner Mongolia Autonomous Region, Inner Mongolia Autonomous Region Incentive Funding Guided Project for Science & Technology Innovation (2016).

Appendix A. Supplementary data

Supplementary material related to this article can be found, in the online version, at doi:https://doi.org/10.1016/j.apcatb.2018.03.086.

References

[1] X.B. Chen, S.H. Shen, L.J. Guo, S.S. Mao, Chem. Rev. 110 (2010) 6503–6570.
[2] J. Zhang, X. Chen, K. Takanabe, K. Maeda, K. Domen, J.D. Epping, X. Fu, M. Antonietti, X. Wang, Angew. Chem. Int. Ed. 49 (2010) 441–444.
[3] X. Wang, K. Maeda, A. Thomas, K. Takanabe, G. Xin, J.M. Carlsson, K. Domen, M. Antonietti, Nat. Mater. 8 (2009) 76–80.
[4] X. Chen, L. Liu, P.Y. Yu, S.S. Mao, Science 331 (2011) 746–750.
[5] X. Lin, Y. Wang, J. Zheng, C. Liu, Y. Yang, G. Che, Dalton Trans. 44 (2015) 19185–19193.
[6] K. Maeda, K. Teramura, D. Lu, T. Takata, N. Saito, Y. Inoue, K. Domen, Nature 440 (2006) 295.
[7] T. Simon, N. Bouchonville, M.J. Berr, A. Vaneski, A. Adrovic, D. Volbers, R. Wyrwich, M. Döblinger, A.S. Susha, A.L. Rogach, F. Jäckel, J.K. Stolarczyk, J. Feldmann, Nat. Mater. 13 (2014) 1013–1018.
[8] J. Liu, Y. Liu, N. Liu, Y. Han, X. Zhang, H. Huang, Y. Lifshitz, S. Lee, Jun Zhong, Z. Kang, Science 347 (2015) 970–974.
[9] S. Cao, J. Low, J. Yu, M. Jaroniec, Adv. Mater. 27 (2015) 2150–2176.
[10] H. Wang, L. Zhang, Z. Chen, J. Hu, S. Li, Z. Wang, J. Liu, X. Wang, Chem. Soc. Rev. 43 (2014) 5234–5244.
[11] J. Zhang, Y. Wang, J. Jin, J. Zhang, Z. Lin, F. Huang, J. Yu, ACS Appl. Mater. Interfaces 5 (2013) 10317–10324.
[12] J. Yu, S. Wang, B. Cheng, Z. Lin, F. Huang, Catal. Sci. Technol. 3 (2013) 1782–1789.
[13] K. Wang, Q. Li, B. Liu, B. Cheng, W. Ho, J. Yu, Appl. Catal. B: Environ. 176–177 (2015) 44–52.
[14] J. Zhang, F. Guo, X. Wang, Adv. Funct. Mater. 23 (2013) 3008–3014.
[15] S. Kang, L. Zhang, C. Yin, Y. Li, L. Cui, Y. Wang, Appl. Catal. B: Environ. 211 (2017) 266–274.
[16] Y. Wang, X. Bai, H. Qin, F. Wang, Y. Li, X. Li, S. Kang, Y. Zuo, L. Cui, ACS Appl. Mater. Interfaces 8 (2016) 17212–17219.
[17] Y. Shiraishi, Y. Kofuji, S. Kanazawa, H. Sakamoto, S. Ichikaw, S. Tanaka, T. Hirai, Chem. Commun. 50 (2014) 15255–15258.
[18] C. Han, L. Wu, L. Ge, Y. Li, Z. Zhao, Carbon 92 (2015) 31–40.
[19] Y. Hou, Y. Zhu, Y. Xu, X. Wang, Appl. Catal. B: Environ. 156–157 (2014) 122–127.
[20] J. Xu, Y. Li, S. Peng, Int. J. Hydrogen Energy 40 (2015) 353–362.
[21] Y. Zhu, Y. Xu, Y. Hou, Z. Ding, X. Wang, Int. J. Hydrogen Energy 39 (2014) 11873–11879.
[22] C.A. Caputo, M.A. Gross, V.W. Lau, C. Cavazza, B.V. Lotsch, E. Reisner, Angew. Chem. Int. Ed. 53 (2014) 11538–11542.
[23] G. Zhang, G. Li, X. Wang, ChemCatChem 7 (2015) 2864–2870.
[24] J. Yang, D. Wang, H. Han, C. Li, Acc. Chem. Res. 46 (2013) 1900–1909.
[25] G. Liu, T. Wang, H. Zhang, X. Meng, D. Hao, K. Chang, P. Li, T. Kako, J. Ye, Angew. Chem. Int. Ed. 54 (2015) 1–6.
[26] Z. Pan, Y. Zheng, F. Guo, P. Niu, X. Wang, ChemSusChem 9 (2016) 1–5.
[27] G. Zhang, S. Zang, X. Wang, ACS Catal. 5 (2015) 941–947.
[28] Y. Shiraishi, Y. Kofuji, H. Sakamoto, S. Tanaka, S. Ichikawa, T. Hirai, ACS Catal. 5 (2015) 3058–3066.
[29] Q. Han, B. Wang, J. Gao, Z. Cheng, Y. Zhao, Z. Zhang, L. Qu, ACS Nano 10 (2016) 2745–2751.
[30] J. Zhang, M. Zhang, R. Sun, X. Wang, Angew. Chem. Int. Ed. 51 (2012) 10145–10149.
[31] Z. Hong, B. Shen, Y. Chen, B. Lin, B. Gao, J. Mater. Chem. A 1 (2013) 11754–11761.
[32] G. Zhang, M. Zhang, X. Ye, X. Qiu, S. Lin, X. Wang, Adv. Mater. 26 (2014) 805–809.
[33] Q. Liang, Z. Li, Z. Huang, F. Kang, Q. Yang, Adv. Funct. Mater. 25 (2015) 6885–6892.
[34] J. Di, J. Xia, X. Li, M. Ji, H. Xu, Z. Chen, H. Li, Carbon 107 (2016) 1–10.
[35] H. Lan, L. Li, X. An, F. Liu, C. Chen, H. Liu, J. Qu, Appl. Catal. B: Environ. 204 (2017) 49–57.
[36] X. Wang, W. Yang, F. Li, Y. Xue, R. Liu, Y. Hao, Ind. Eng. Chem. Res. 52 (2013) 17140–17150.
[37] X. Zhou, B. Jin, L. Li, F. Li, H. Peng, H. Wang, Y. Yu, J. Fang, Mater. Chem. 22 (2012) 17900–17905.
[38] B. Chai, T. Peng, J. Mao, K. Li, L. Zan, Phys. Chem. Chem. Phys. 14 (2012) 16745–16752.